Applied Catalysis B: Environmental 138–139 (2013) 17–25

Contents lists available at SciVerse ScienceDirect

Applied Catalysis B: Environmental

journal homepage: www.elsevier.com/locate/apcatb

Multifunctional graphene oxide–TiO_2 microsphere hierarchical membrane for clean water production

Peng Gao[a,b], Zhaoyang Liu[a,*], Minghang Tai[a], Darren Delai Sun[a,**], Wunjern Ng[a,b]

[a] School of Civil and Environmental Engineering, Nanyang Technological University, 50 Nanyang Avenue, Singapore 639798, Singapore
[b] Nanyang Environment & Water Research Institute, Nanyang Technological University, 50 Nanyang Avenue, Singapore 639798, Singapore

ARTICLE INFO

Article history:
Received 21 October 2012
Received in revised form 5 January 2013
Accepted 14 January 2013
Available online 23 January 2013

Keywords:
Hierarchical membrane
Multifunction
Anti-fouling
Water production

ABSTRACT

The severe scarcity of clean water is arousing concern worldwide. The development of clean water production heavily relies on membrane technology, although the performance of current membranes is significantly restricted by membrane fouling. In this work, a novel graphene oxide (GO)–TiO_2 microsphere hierarchical membrane was fabricated through assembling GO–TiO_2 microsphere composite on the surface of a polymer filtration membrane. This kind of membrane possesses the multifunction of concurrent water filtration and degradation of pollutants. GO sheets play double roles in GO–TiO_2 membrane, including (1) cross linker for individual TiO_2 microspheres; and (2) electron acceptor to enhance photocatalytic activity. Hence, this novel membrane shows sustainably high permeate flux due to the hierarchical membrane structure, high photodegradation activity and no membrane fouling. The excellent performance of this GO–TiO_2 hierarchical membrane indicates its promising potential in clean water production field.

1. Introduction

The development of the world economy heavily relies on clean water. Nowadays, scarcity of drinking water has become one of the most severe worldwide problems [1]. However, the various contaminants, including natural organic matters, industrial dyes, microorganisms and heavy metals, further worsen this problem [2–4]. Recently, there is a trend in the use of membrane technology for production of safe drinking water [5–7]. Although extant polymer membrane can perform efficient and selective separations in many water treatment fields including industrial waste water reclamation and desalination, some problems associated with membrane properties and membrane treatment processes, such as low flux, low selectivity and fouling still remain significant challenges. Among them, membrane fouling poses a major obstacle that requires further improvements in the membrane performance [8,9]. In recent years, ceramic membranes have attracted intensive research interests in view of their higher mechanical strength, enhanced chemical stability and excellent performance in the removal of pollutants to eliminate fouling problems [10,11].

Titania, in particular, anatase TiO_2, has been widely used to fabricate ceramic membrane due to its unique properties [11–13]. TiO_2 membrane is an ideal substitute of polymer membrane, as it can achieve concurrent water filtration and photocatalytic degradation of pollutant, which greatly alleviates membrane fouling [14,15]. Up to date, various TiO_2 nanoarchitectures, including nanowire [11,14], nanofiber [16–18] and microsphere [13,15], have been applied to fabricate membrane. Zhang et al. fabricated a TiO_2 nanowire ultrafiltration membrane with a layered hierarchical structure and concluded that this UF membrane offered three major advantages, including high permeability and selectivity, concurrent photocatalytic oxidation and separation, and antifouling as well as antibacterial capacity [11]. In addition, Choi et al. prepared nanostructured crystalline TiO_2 thin films and TiO_2/Al_2O_3 composite membranes through a simple sol–gel route and demonstrated that the photocatalytic TiO_2 membrane displayed excellent performances, including high water permeability, sharp polyethylene glycol retention, high efficient in inactivation of *E. coli* and less fouling tendency [19]. Furthermore, in the previous work of our group, hierarchically mesoporous F-TiO_2 hollow microspherical membrane had been used for water purification and exhibited improved anti-fouling property [15]. However, some problems related to these TiO_2 membranes still remain unresolved. Firstly, no connection was formed between the materials making the membrane easily broken. In addition, drying and calcination processes usually introduce the pinholes and cracks into the membrane [20]. Furthermore, pure TiO_2 membrane is not efficient for photodegradation of pollutant due to the rapid charge recombination rate [21]. Hence, there is an urgent need to develop a facile method to fabricate a novel membrane with anti-fouling property to overcome above drawbacks.

* Corresponding author. Tel.: +65 82987689.
** Corresponding author. Tel.: +65 67906273; fax: +65 6791 0676.
E-mail addresses: ZYLIU@ntu.edu.sg (Z. Liu), DDSUN@ntu.edu.sg (D.D. Sun).

0926-3373/$ – see front matter © 2013 Elsevier B.V. All rights reserved.
http://dx.doi.org/10.1016/j.apcatb.2013.01.014

Graphene is a single atomic thick sheet of graphite and can be regarded as unrolled CNT, which attracts tremendous research attentions since it is discovered by Novoselov and Geim [22]. Graphene oxide (GO) is a chemically modified graphene with epoxide and phenol hydroxyl groups on its basal plane and carboxylic groups at its edges [23,24]. Until now, researchers have prepared significant amount of GO and TiO_2 composites through various methods and GO–TiO_2 composites have shown enhanced activities as photocatalysts, solar cells and LIBs [24–29]. Therefore, a practical way to conquer the problems of current TiO_2 membrane is adopting GO sheets as cross linkers to form joints between individual TiO_2 particle, wire or sphere.

In this study, we report a new type of GO–TiO_2 microsphere membrane for concurrent water filtration and photodegradation. This novel membrane is consisted of hierarchical TiO_2 microspheres and GO sheets, in which GO sheets serve as binders for individual TiO_2 microspheres. Compared with previous ceramic membranes, GO–TiO_2 microsphere membrane possesses two major advantages: (1) sustainably high water flux due to alleviation of membrane fouling by the hierarchically porous membrane structure; and (2) enhanced strength and flexibility from the cross-linking effect of GO sheets.

2. Experimental methods

2.1. Materials

Tetrabutyl titanate (TBT), acetic acid (HAc), sodium nitrate ($NaNO_3$, 99%), potassium permanganate ($KMnO_4$, 99%), hydrogen peroxide (H_2O_2, 35%), concentrated sulfuric acid (H_2SO_4, 98%), hydrochloric acid (HCl, 37%), rhodamine B (RhB) and acid orange 7 (AO7) were obtained from Sigma–Aldrich. Humic acid (HA) was purchased from Fluka Company. In addition, natural graphite (SP1) was obtained from Bay Carbon Company (USA). All chemicals were used without further purification. Furthermore, deionized (DI) water was produced from Millipore Milli-Q water purification system.

2.2. Synthesis of GO

GO was prepared according to the modification of Hummer's method [30], and the procedure was described previously [23,31].

2.3. Synthesis of TiO_2 microsphere

TiO_2 microsphere was synthesized by the reported method with slight modification [32]. Typically, 1 mL of TBT was added dropwise to 35 mL of HAc with continuous stirring for 10 min. Thereafter, the obtained white suspension was transferred to a 45 mL Teflon-lined stainless-steel autoclave, which was then heated to 180 °C and kept for 6 h. The product was collected by centrifugation after the autoclave cooled to room temperature and followed by ethanol washing. Finally, the material was dried at 60 °C for 24 h and calcined at 500 °C for 2 h to obtain anatase TiO_2 phase with a ramping rate of 2 °C min^{-1}.

2.4. Synthesis of GO–TiO_2

GO–TiO_2 was prepared according to our previous report [24]. In a typical process, 10 mg of as synthesized GO was well dissolved in 100 mL of DI water. Then, 200 mg of as prepared TiO_2 microsphere was added to GO solution. The mixture was first put under ultrasonic condition for 30 min and then kept stirring for 2 h. Finally, the mixture was centrifuged and put into vacuum drier for further usage.

2.5. Assembly of GO–TiO_2 membrane

200 mg of as synthesized GO–TiO_2 was dissolved into 100 mL of DI water to form uniform suspension. Then, the suspension was injected into the filtration cup with one piece of commercial cellulose acetate (CA) membrane (Φ 47 mm, 0.45 μm, Millipore, USA) on the bottom of the cup. GO–TiO_2 membrane was uniformly assembled on the surface of CA membrane after switching on the nitrogen gas for 30 min.

For comparison, P25 membrane and TiO_2 microsphere membrane were also fabricated using 200 mg of P25 and TiO_2 microsphere as raw materials, respectively.

2.6. Characterization

The structure and crystal phase of GO, TiO_2 microsphere and GO–TiO_2 were examined by X-ray diffraction (XRD, Shimadzu XRD-6000) with monochromated high-intensity Cu Kα radiation (λ = 1.5418 Å) operated at 40 kV and 30 mA. Surface topography of GO sheets was characterized by atomic force microscopy (AFM, PSIA XE-150). The morphologies of TiO_2 microsphere and GO–TiO_2 were evaluated by field emission scanning electron microscopy (FESEM, JSM-7600F). Transmission electron microscopy (TEM) and high-resolution TEM (HRTEM) images of TiO_2 microsphere and GO–TiO_2 were acquired using a JEOL 2010-H microscope (TEM) operating at 200 kV. In addition, the Brunauer-Emmet-Teller (BET) specific surface area of GO–TiO_2 was determined at liquid nitrogen temperature (77 K) using the Micromeritics ASAP 2040 system. The pore size distribution is calculated from the desorption branch of the isotherm according to the BJH model. Photoluminescence (PL) spectra were measured on the spectrofluorophotometer (Shimadzu RF-5301). Furthermore, the adsorption values of the RhB and AO7 at wavelength of 552 nm [16] and 485 nm [33], respectively, were measured by UV–vis spectrometer (UV-visible resource 3000), while the total organic carbon (TOC) concentration of HA was measured by a Shimadzu TOC-VCSH TOC analyzer.

2.7. Investigation of membrane flux

The flux performance of GO–TiO_2 membrane was tested in a dead-end membrane system setup without UV light irradiation, which had been reported by our group, as shown in Fig. 4 [13]. As contrasts, P25 membrane and TiO_2 microsphere membrane were also investigated under the same condition. In addition, the flux of CA membrane was recorded as control. This bench-scale system comprises of a membrane cell with a filtration cup volume of 60 mL and the effective membrane area is 11.94 cm^2. Working pressure was provided by N_2 gas cylinder, which was connected to the filtration cup. The weight of permeate was measured continuously over time using a balance, which was connected to the data logger. Furthermore, data was collected every ten second and then averaged each 10 min. Permeate flux was calculated on the basis of permeate mass divided by effective surface area and filtration time, unit is L/(m^2 h). The membrane flux was investigated under different trans-membrane pressure (TMP). In addition, these membranes were pre-compressed under pressure of 2 bar for 6 h to exclude the interference of membrane swelling [34].

2.8. Photodegradation activity of GO–TiO_2 membrane

The photodegradation activity of GO–TiO_2 membrane was evaluated using RhB and AO7 as model pollutants. The same dead-end membrane filtration setup was used with UV light irradiation (254 nm, 40 mW/cm^2), as shown in Fig. 4. For the photodegradation of RhB, 50 mL of RhB solution with concentration of 50 mg/L (50 ppm) was filled into the filtration cup. UV light was turned on

after the solution was kept in dark for 60 min to reach adsorption equilibrium. The TMP was maintained about 0.5 bar within the whole process. 2 mL permeate were collected to measure the UV adsorption at an interval of 5 min within 30 min. In addition, 50 mL of AO7 with concentration of 50 mg/L was also investigated under the same condition.

As references, CA membrane, P25 membrane and TiO_2 microsphere membrane were investigated under the same processes.

2.9. Anti-fouling property of GO–TiO_2 membrane

200 mg of GO–TiO_2 materials were well assembled on one piece of CA membrane. Then, HA feed water with concentration of 20 mg/L was permeated through GO–TiO_2 membrane under pressure (2 bar) provided by N_2 gas, with or without UV irradiation. The permeate flux was calculated and TOC of permeate was measured within certain time. In comparison with GO–TiO_2 membrane, anti-fouling activities of CA membrane, P25 membrane and TiO_2 microsphere membrane were also investigated under the same condition.

3. Results and discussion

3.1. Morphology and structure properties of GO–TiO_2 membrane

The surface morphology of well synthesized GO sheets was characterized by AFM. Fig. 1a shows single layered GO sheets with some overlap are successfully synthesized and the typical size of GO sheets is more than 2 μm. In addition, as shown in Fig. 1b, the thickness of single layered GO sheets is around 0.9 nm from the two line scans and three dimensional (3D) image of AFM, which is similar with the previous reports [35,36]. Fig. 1c and d exhibits FESEM images of TiO_2 microsphere, which is synthesized from solvothermal method. The relatively uniform flower-like TiO_2 microsphere was successfully prepared, as shown in Fig. 1c. Fig. 1d is the high magnification of one TiO_2 microsphere, the size of which is around 2.5 μm. In addition, TiO_2 microsphere is assembled by numerous nanorods and nanosheets, which grow along the radial direction. To better analyze TiO_2 microsphere, the microstructures of TiO_2 microsphere were characterized with TEM. TEM images at low and high magnifications are displayed in Fig. 1e and inset. TEM image shows TiO_2 microsphere is solid structure with a typical size of 2.5 μm, which confirms the results of FESEM. A closer observation of the edge of TiO_2 microsphere indicates that the microspheres are in fact constructed from nanorods, while these nanorods are assembled by highly crystalline nanoparticles, as shown in Fig. 1e. Furthermore, to confirm the crystallization of TiO_2 microsphere, a high resolution TEM (HRTEM) image was taken from two nanorods at the edge of the microsphere. As shown in Fig. 1f, the clear lattice-fringe with inter-plane spacing of 0.34 nm is attributed to the (1 0 1) crystal plane of the anatase TiO_2, which confirms that TiO_2 microsphere is composed of highly crystallized anatase [37]. The high crystalline anatase TiO_2 microsphere can enhance the charge transfer and photodegradation activity [38–40]. Based on the analyses of AFM, FESEM and TEM, GO sheets and TiO_2 microsphere were successfully synthesized in our experiments.

The structures of GO–TiO_2 were well characterized by FESEM and TEM. Fig. 2a shows several TiO_2 microspheres are bound together by GO sheets. In addition, the surface of some microspheres are wholly wrapped by GO, which can be clearly seen from Fig. 2a. As shown in Fig. 2b, the edges of two TiO_2 microspheres are connected by GO sheets, in which GO act as "bridges" to chemically bond with TiO_2 [16]. TEM is a powerful method to analyze GO based composites because GO sheets sometimes cannot be clearly observed under SEM [41]. Fig. 2c shows one TiO_2 microsphere connected with GO sheets. The edge of GO–TiO_2 is blurry and nanorod structure cannot be seen clearly, which is different from that of TiO_2 microsphere (inset of Fig. 1e). This is because GO sheets are attached on the surface and edge of TiO_2 microsphere. Fig. 2d is the higher magnification of red frame in Fig. 2c. As shown in Fig. 2d, GO sheets bond with the edge of TiO_2 microsphere can be clearly identified. Hence, the results of FESEM and TEM characterization provide strong evidences that GO–TiO_2 was successfully prepared, in which TiO_2 microspheres were bonded together with the help of GO sheets. This structure is beneficial for membrane fabrication because GO can enhance the connection between dispersive TiO_2 microsphere and improve the strength of membrane, as well as the flexibility. In addition, strong contact between GO sheets and TiO_2 microspheres can enhance the charge transfer and thereafter the photodegradation activity during concurrent water filtration and photodegradation process, which will be discussed in detail later.

XRD patterns of GO, TiO_2 microsphere and GO–TiO_2 are shown in Fig. 3a, respectively. The diffraction peak of GO at 2θ of 11.9° can be attributed to interlamellar water trapped between GO sheets [42]. In addition, the diffraction peaks at 2θ of 25.3, 38.2, 48.1, 53.5, 55.6, 62.7 and 75.0° are attributed to anatase TiO_2 (JCPDF 21-1272). GO–TiO_2 shows similar diffraction peaks with TiO_2 microsphere, while no peaks of GO are observed because the regular stack of GO sheets is destroyed by intercalation of TiO_2 microsphere [24].

Another benefit of choosing GO–TiO_2 microsphere to fabricate membrane is the large BET surface area and porous structure, which is essential to achieve high water flux and photodegradation efficiency. Fig. 3b shows N_2 adsorption–desorption isotherms of GO–TiO_2. The BET surface area of GO–TiO_2 is 107.57 $m^2\ g^{-1}$, which is greatly larger than that of P25 (45 $m^2\ g^{-1}$). Major pore size distribution of GO–TiO_2 is ranged from 10 to 40 nm with a peak around 20 nm, which is a typical mesoporous structure, as shown in the inset of Fig. 3b. The mesoporous structure with such big surface area provides more channels for water molecule to go through and enhances the photogenerated electrons and holes to participate in photocatalytic activity [15,37].

3.2. Water filtration property of GO–TiO_2 membrane

To demonstrate the engineering applicability of GO–TiO_2 membrane for water purification, the flux performance of GO–TiO_2 membrane was investigated in a lab-scale dead end set up, as shown in Fig. 4. As contrasts, the water filtration activity of control CA membrane, P25 membrane and TiO_2 microsphere membrane were also tested. In addition, steady permeate flux was achieved by pre-compressed these membranes under pressure of 2 bar for 6 h to exclude the interference of membrane swelling [34]. Fig. 5a shows the pure water flux of control CA membrane, P25 membrane, TiO_2 microsphere membrane and GO–TiO_2 membrane, respectively, while the same mass of 200 mg of P25, TiO_2 microsphere and GO–TiO_2 are well deposited on CA membrane surface. As shown in Fig. 5a, permeate flux of all these membranes increases linearly with TMP, indicating that these membranes are incompressible and only intrinsic membrane resistances (R_m) are present in these experiments [43]. In addition, the flux of TiO_2 microsphere membrane and GO–TiO_2 membrane is significantly larger than that of P25 membrane, which can be explained by Fig. 6 Fig. 6 shows the schematic diagram (left side) and surface morphology (right side) of P25 membrane, TiO_2 microsphere membrane and GO–TiO_2 membrane, individually. As shown in Fig. 6a, P25 nanoparticle with size around 20 nm prefer to form an extremely dense layer on the surface of polymer membrane and some particles are likely to block the pore of CA membrane, resulting of low flux even at high TMP [15]. However, TiO_2 microsphere membrane and GO–TiO_2 membrane form more porous structure due to the large size of individual

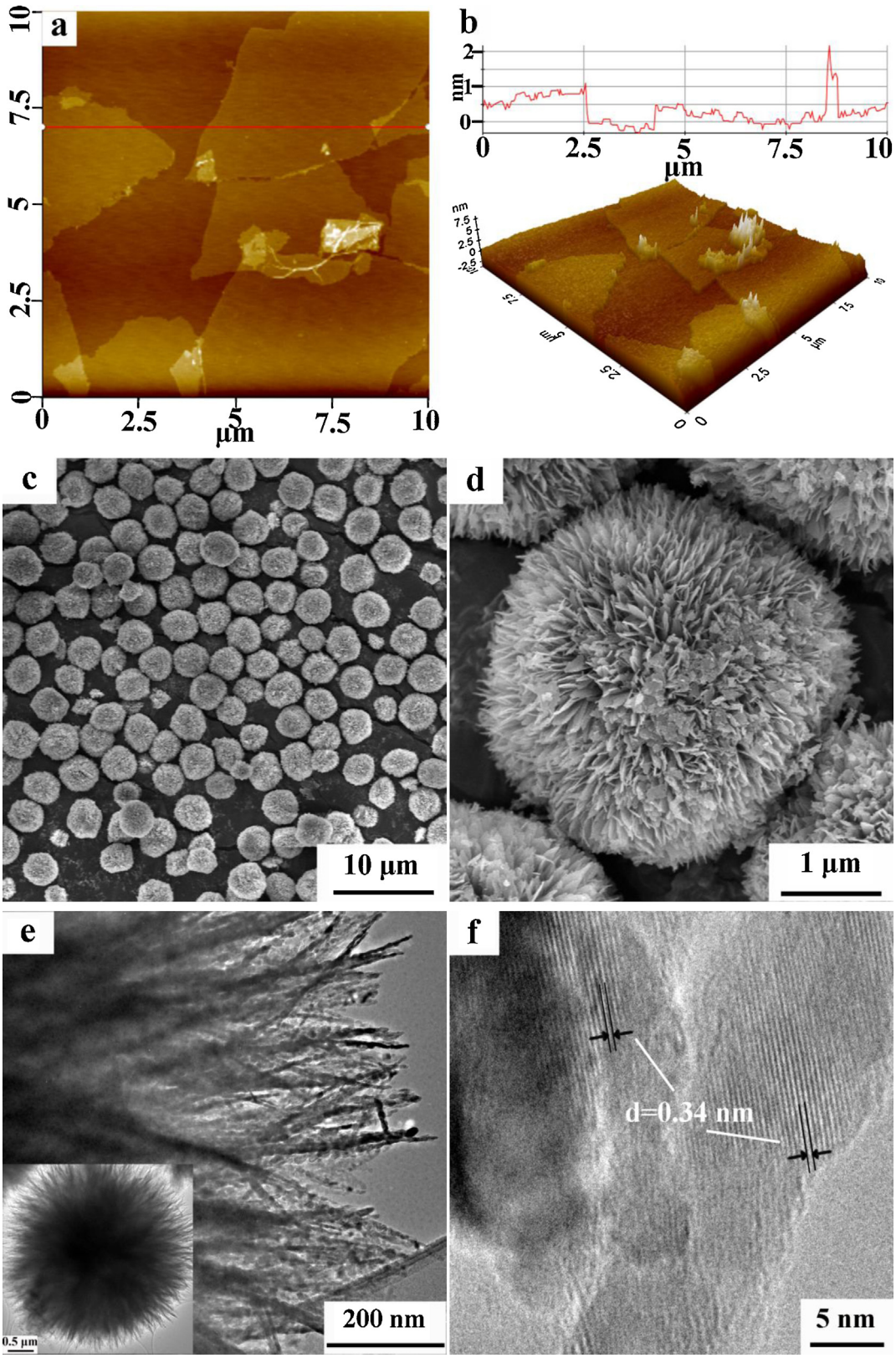

Fig. 1. (a) 2D AFM image of GO sheets; (b) two line scan and 3D AFM image of GO sheets; (c) and (d) FESEM images of TiO_2 microsphere; (e) TEM images of one whole TiO_2 microsphere (inset) and the edge; and (f) HRTEM image of TiO_2 microsphere.

TiO_2 microsphere with porous property. In addition, as expected, the permeate flux of GO–TiO_2 membrane is slightly lower than that of TiO_2 microsphere membrane because the presence of GO sheets. GO sheets can reduce the both inter- and intra-pore of GO–TiO_2 membrane, which is beneficial for high separation efficiency [44]. It is well known that membrane with high flux and separation efficiency is ideal in water treatment fields, since more high quality water will be produced at a low cost. In this respect, GO–TiO_2

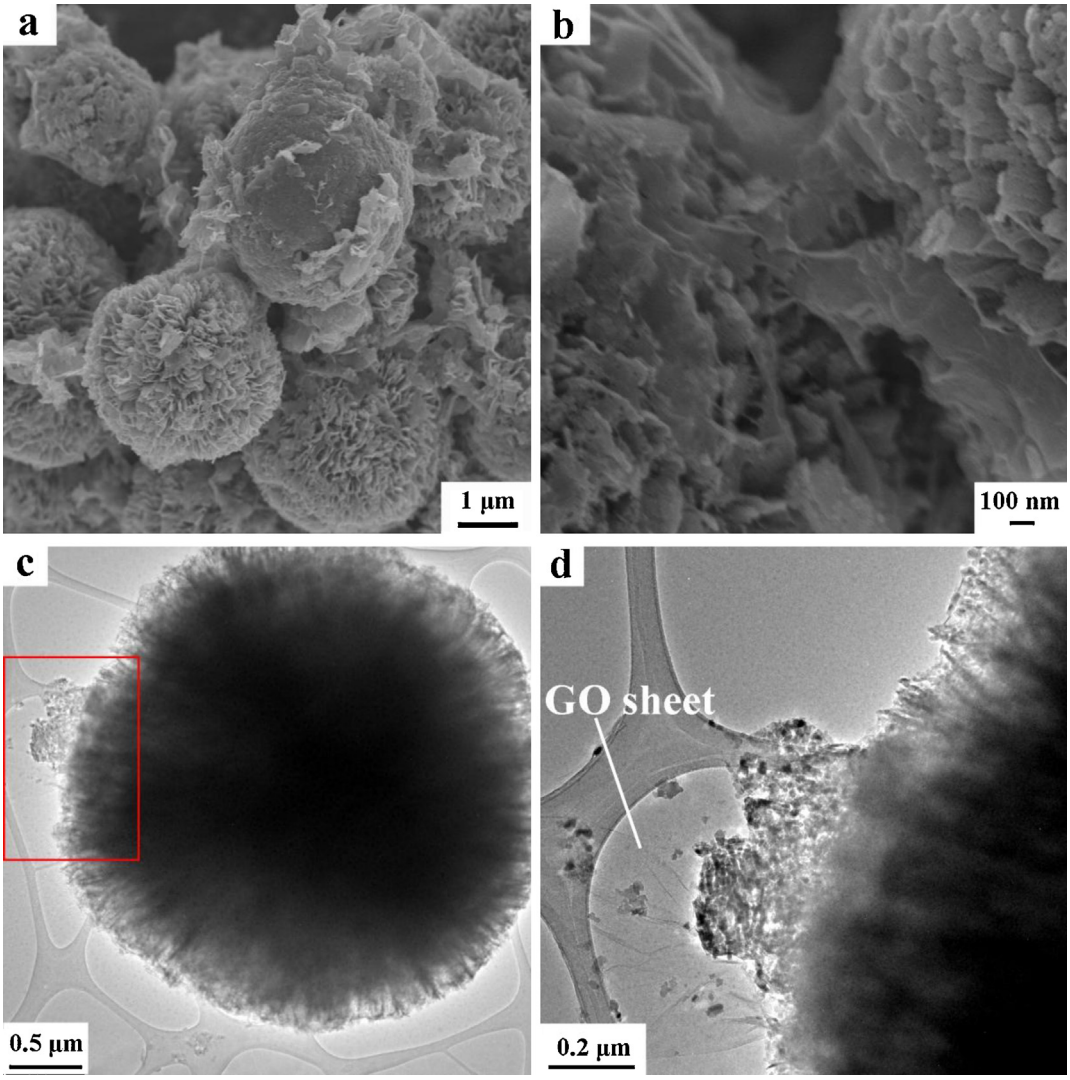

Fig. 2. (a) FESEM images of GO–TiO_2; (b) FESEM image of GO sheets connecting the edges of two TiO_2 microspheres; (c) TEM image of GO–TiO_2; and (d) high magnification image of red frame in (c).

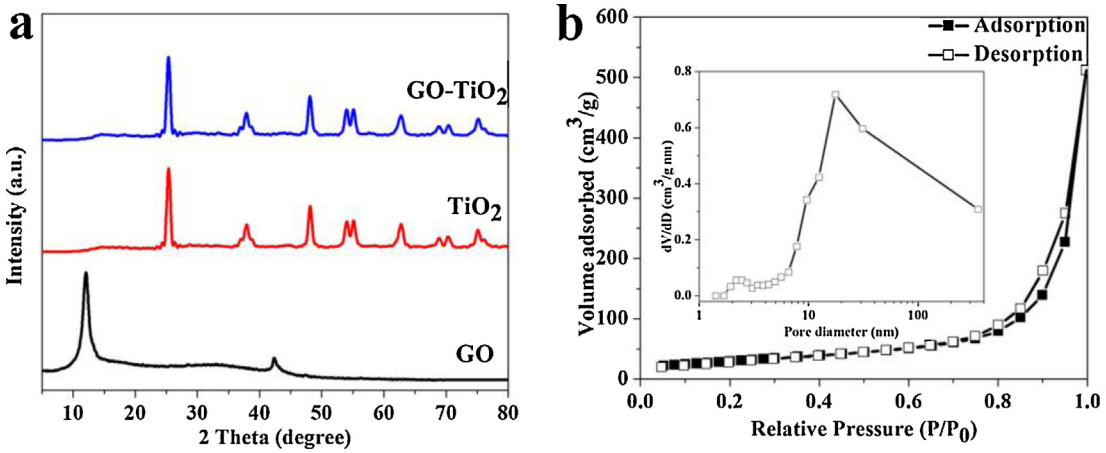

Fig. 3. (a) XRD patterns of GO, TiO_2 microsphere and GO–TiO_2 microsphere, respectively; and (b) N_2 adsorption/desorption isotherm of GO–TiO_2 (inset: pore size distribution).

membrane shows bright future in water purification field. Furthermore, the thickness of GO–TiO_2 membrane can be easily adjusted through changing the mass of GO–TiO_2 deposited on the surface of CA membrane, while the thickness has little influence on the permeate flux because the porous structure of GO–TiO_2 membrane, as shown in Fig. 5b.

Another significant advantage of GO–TiO_2 membrane than tradition TiO_2 membrane is enhanced strength and flexibility. As

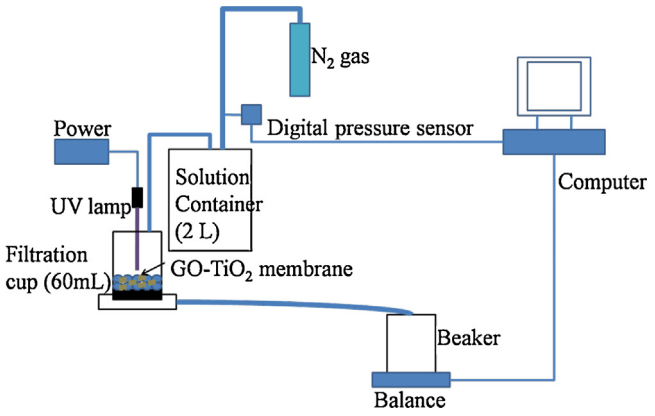

Fig. 4. Schematic diagram of lab-scale dead end water filtration setup.

shown in Supplementary Fig. S1 and inset of Fig. 6c (right side), GO–TiO_2 membrane remains as intact with good flexibility after dry and no obvious cracks can be found, while TiO_2 microsphere membrane is totally broken into several pieces after dry due to lack of linkage between dispersive TiO_2 microsphere (right side of Fig. 6b, inset). According to our understanding, high strength and flexibility is imperative in water filtration industry because membrane usually works under high pressure. Hence, GO–TiO_2 membrane has promising potential to be used in real water treatment industry.

3.3. Photodegradation activity of GO–TiO_2 membrane

The photodegradation activity of GO–TiO_2 membrane was investigated by degradation of RhB and AO7, which are the major pollutants from textile industries. CA membrane, P25 membrane and TiO_2 microsphere membrane were also tested as references under the same condition. Supplementary Fig. S2a and b shows the removal rate of RhB and AO7 dye in the process of membrane filtration alone and UV light irradiation alone, respectively. As shown in Supplementary Fig. S2a, the GO–TiO_2 membrane itself has limited efficiency in removing dyes and less than 15% of RhB and AO7 can be removed by membrane filtration process without UV irradiation. This is because GO–TiO_2 membrane is only a common filter without UV light and the concentration reduction of dyes is attributed to the adsorption activity of GO–TiO_2 membrane. Supplementary Fig. S2b shows that UV light itself can only degrade less than 50% of RhB and AO7. As shown in Fig. 7a and b, GO–TiO_2 membrane shows higher photodegradation efficiency towards both RhB and AO7 dyes than P25 and TiO_2 microsphere membrane. RhB and AO7 dyes are totally degraded within 30 and 20 min by GO–TiO_2 membrane under UV irradiation, respectively. The efficient photocatalytic activity plays a significant role in eliminating membrane fouling, because less organics and macromolecules can be accumulated on the GO–TiO_2 membrane surface, which guarantees GO–TiO_2 membrane can maintain high permeate flux for longer time than traditional membranes.

3.4. Anti-fouling property of GO–TiO_2 membrane

Fabricating membrane with anti-fouling property is an urgent need for water purification industry due to the high cost for cleaning membrane fouling. The anti-fouling capacity of CA membrane, P25 membrane, TiO_2 microsphere membrane and GO–TiO_2 membrane were investigated by choosing HA as a standard pollutant, which is a typical natural organic matter (NOM) in water and the precursor of carcinogenic disinfection by-products (DBPs) [45]. Membranes used for anti-fouling test should be firstly precompacted under pressure of 2 bar for 6 h to eliminate the influence of initial flux decline and confirm that decrease of flux is solely caused by HA fouling [34]. Fig. 8a shows the time courses of permeate flux without UV light irradiation, in the presence of control CA membrane, P25 membrane, TiO_2 microsphere membrane and GO–TiO_2 membrane, respectively. Remarkably rapid drop of flux for all membranes can be observed in the first 30 min, as shown in Fig. 8a. This can be attributed to the large HA particles or aggregates were rapidly deposited on the surface of membrane and blocked the pores at the initial stage of filtration [43]. In addition, significant membrane fouling was occurred after 2 h and stably small flux (ca. 7 L/(m^2 h)) was reached because thick HA cake layer was formed on the surface of membrane [46]. Nevertheless, membrane fouling can be greatly reduced with UV irradiation. As shown in Fig. 8b, the permeate flux of CA membrane still declines relatively fast, indicating the efficiency of UV irradiation itself is limited. Compared with Fig. 8a, the permeate flux of both GO–TiO_2 membrane and TiO_2 microsphere membrane can keep at a high value for a relative long time, while the flux of GO–TiO_2 membrane is higher than that of TiO_2 microsphere membrane. The permeate flux of GO–TiO_2 membrane (ca. 60 L/(m^2 h)) is around 9 times higher than that of CA and P25 membrane at the steady state. In addition, no obvious decline of flux can be observed even within 15 h because most of HA was photodegraded into small molecules, including carbon dioxide (CO_2) and water (H_2O) [14], by GO–TiO_2 under UV irradiation, which can be verified by the results of TOC analysis.

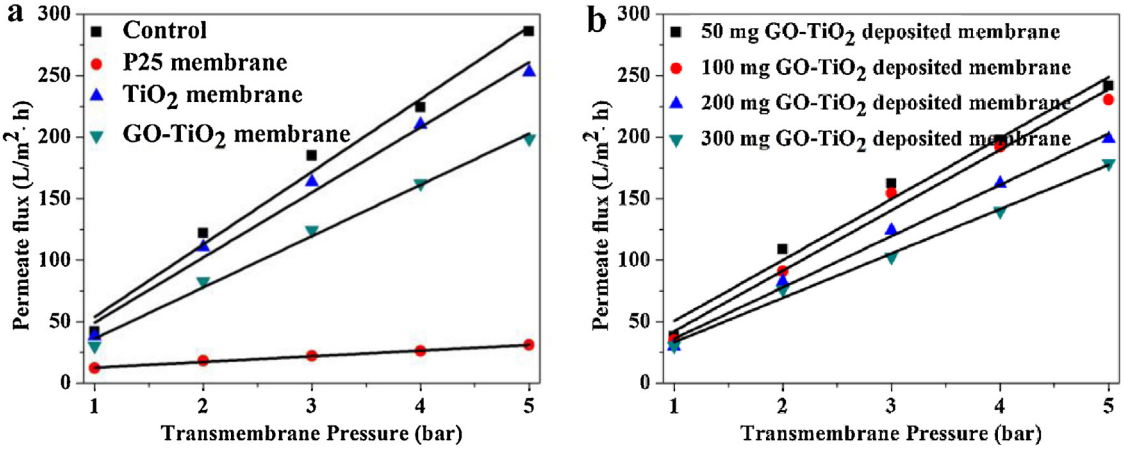

Fig. 5. (a) Changes in permeate flux of control (CA membrane), P25, TiO_2 microsphere and GO–TiO_2 membrane with different TMP, respectively; and (b) influence of thickness of GO–TiO_2 membrane on permeate flux under different TMP.

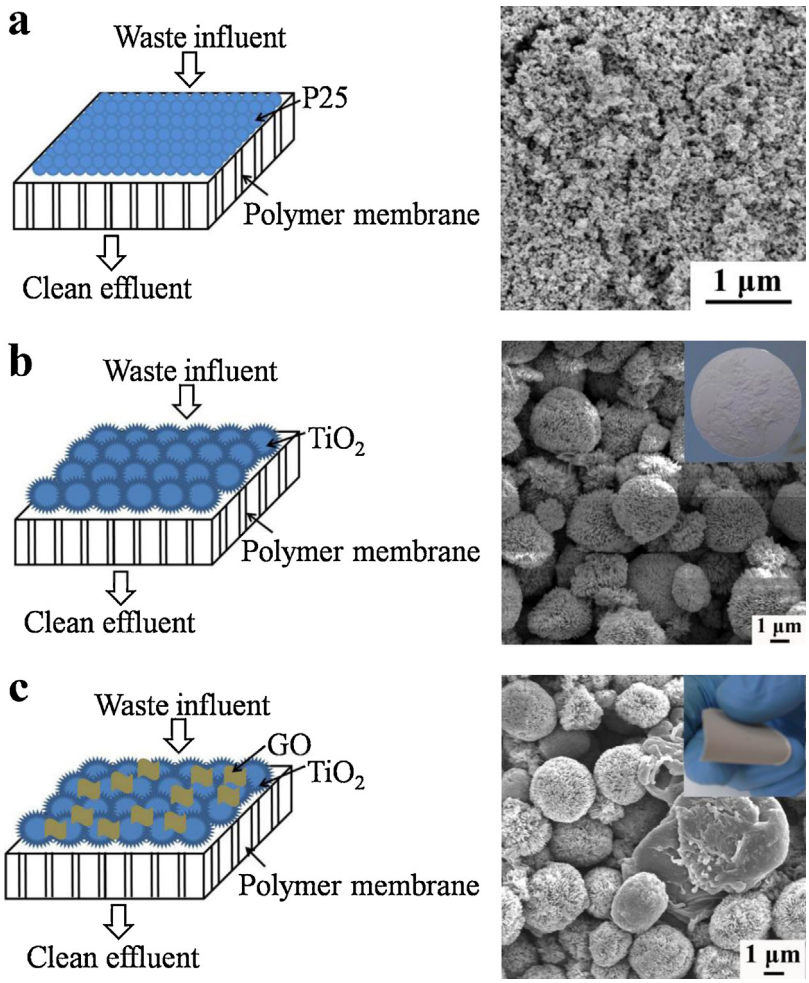

Fig. 6. (a) Schematic diagram of P25 membrane (left side) and FESEM image of P25 membrane surface (right side); (b) schematic diagram of TiO_2 microsphere membrane (left side) and FESEM image of TiO_2 microsphere membrane surface (right side (inset: digital photo of TiO_2 microsphere membrane); and (c) schematic diagram of GO–TiO_2 membrane (left side) and FESEM image of GO–TiO_2 membrane surface (right side (inset: digital photo of GO–TiO_2 membrane).

Fig. 9a shows residual TOC rate of HA from the water permeated through CA, P25, TiO_2 microsphere and GO–TiO_2 membrane, individually. Combining CA membrane with UV irradiation exhibits limited efficiency in removing HA, while GO–TiO_2 membrane shows the highest efficiency and over 90% TOC has been eliminated, which contributes to high flux within a long time. This indicates that most of HA rejected on the membrane surface could be degraded under the current permeate flux (ca. 60 L/(m^2 h)) because the amount of HA did not exceed the maximal photocatalytic capacity of GO–TiO_2 membrane [14]. However, it should be noted that if higher concentration of HA or higher TMP were adopted, the HA might not be degraded effectively and would cause membrane fouling, which would be investigated and improved in the future study. In this work, the enhanced TOC removal efficiency of GO–TiO_2 membrane than CA, P25 and TiO_2 microsphere membrane can be attributed to (1) high specific BET surface area and

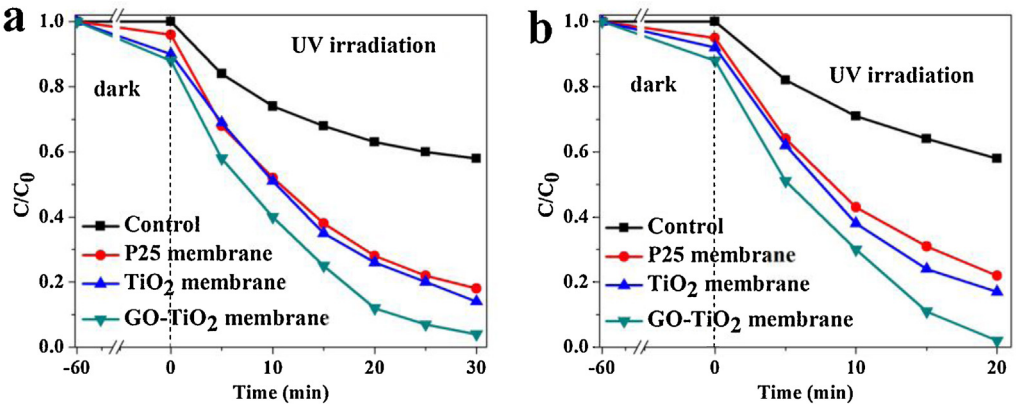

Fig. 7. (a) and (b) Photodegradation of RhB and AO7 in the presence of CA membrane, P25, TiO_2 microsphere and GO–TiO_2 membrane, respectively.

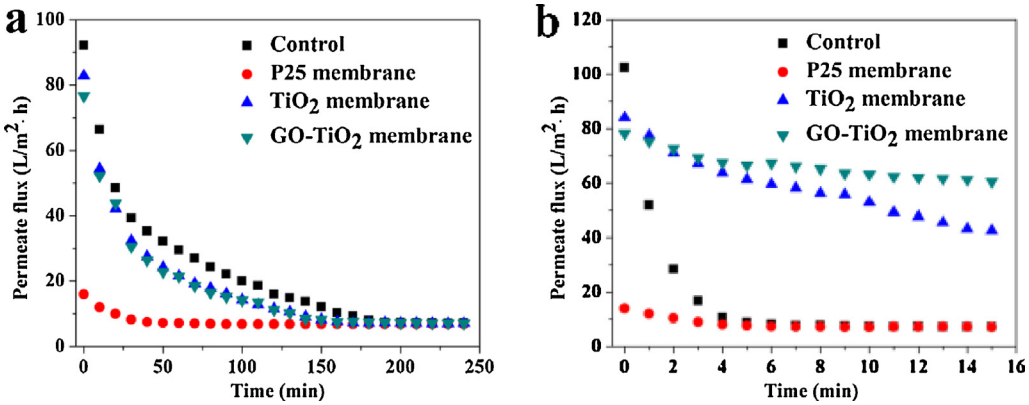

Fig. 8. (a) Changes of permeate flux of different membrane with time under pressure of 2 bar without UV irradiation; and (b) changes of permeate flux of different membrane with time under pressure of 2 bar with UV irradiation.

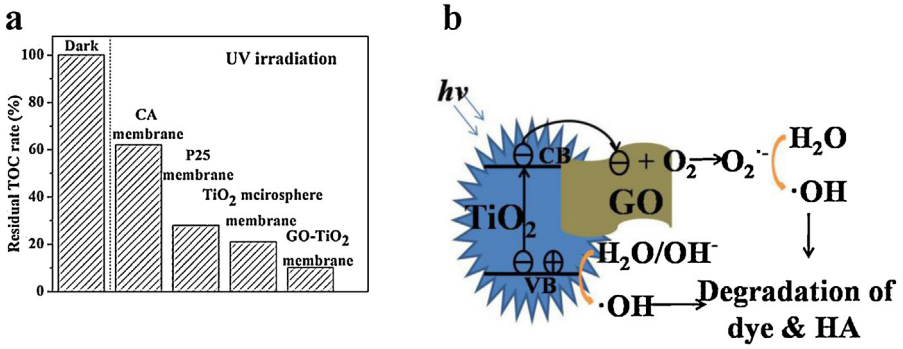

Fig. 9. (a) Residual TOC rate in permeate water filtrated through different membrane; and (b) schematic illustration of mechanism in photodegradation process of GO–TiO_2 membrane.

porous structure; and (2) good contact between GO sheets and TiO_2 microsphere improves the electron transfer from conduction band (CB) of TiO_2 to GO sheets, which reduces the charge recombination rate and enhances the photocatalytic activity, as exhibited in Fig. 9b. shows that connections between GO sheets and TiO_2 microsphere can facilitate the charge transfer. In addition, electrons and holes react with absorbed O_2 and H_2O molecules, respectively, to form hydroxyl radicals (•OH) for further effective photodegradation of dyes and HA [24]. The efficient charge separation process was confirmed by PL spectra. Fig. S3 shows the PL spectra of pure TiO_2 microsphere and GO–TiO_2 composite, respectively. PL emission is originated from the recombination of free charge carriers so the intensity of PL indicates the charge recombination and transfer efficiency in semiconductors [47–49]. The PL intensity of GO–TiO_2 is significant lower than that of TiO_2 microsphere, demonstrating that charge recombination rate is reduced after combining TiO_2 microsphere with GO sheets [48]. This result indicates that photo-generated electrons of TiO_2 microsphere efficiently transfer to GO sheets, while photo-generated holes remain on TiO_2 microsphere, which enhance the charge separation efficiency.

Fig. 10a and b shows FESEM images of surface of GO–TiO_2 membrane after filtration in the absence and presence of UV

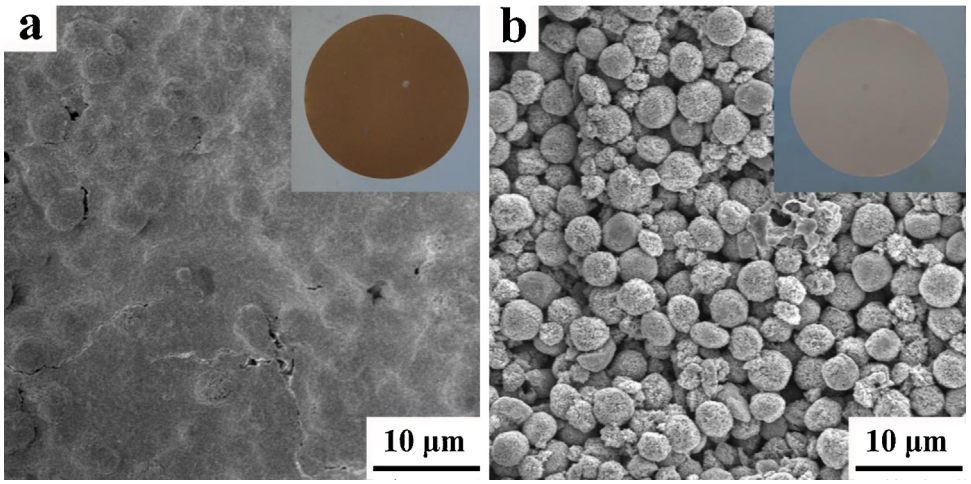

Fig. 10. FESEM images of GO–TiO2 membrane surface after filtration: (a) membrane surface without UV irradiation (inset: digital photo of GO–TiO_2 membrane); and (b) membrane surface with UV irradiation (inset: digital photo of GO–TiO_2 membrane).

irradiation, respectively. Undoubtedly, an extremely dense HA layer was formed on the surface of GO–TiO_2 membrane without UV irradiation, which resulted in low permeate flux in the later period of filtration process. The inset image of Fig. 10a also shows that a brown layer is formed on the initial grey surface of GO–TiO_2 membrane (inset of Fig. 10b), confirming the formation of serious fouling layer during the filtration of HA solution. In addition, the appearance of GO–TiO_2 membrane still can be identified under the HA layer. However, under UV irradiation condition, almost no HA layer can be found on the surface of GO–TiO_2 membrane, indicating that GO–TiO_2 membrane can effectively eliminate membrane fouling with the help of UV light. Consequently, based on the results of permeate flux, photocatalytic activity, fouling as well as the properties of membrane itself (strength and flexibility), GO–TiO_2 membrane shows superior properties and activities than other membranes in our experiments. Enhanced strength and flexibility of GO–TiO_2 membrane can be attributed to the fact that high strength and flexible GO sheets acts as binders between TiO_2 microspheres to prevent membrane from rupture. In addition, flexible membrane can be applied to more water filtration fields due to its better adaptability, so the GO sheets play an indispensable role in GO–TiO_2 membrane.

4. Conclusion

In summary, a novel multifunctional GO–TiO_2 microsphere membrane was successfully prepared for concurrent water filtration and photodegradation. This kind membrane possesses several advantages compared with traditional membranes, including (1) enhanced strength and flexibility; (2) high photodegradation efficiency; (3) high water flux; and (4) anti-fouling. All these excellent properties indicate that GO–TiO_2 microsphere membrane has a bright future in the clean water production field.

Acknowledgements

Authors would like to acknowledge the Clean Energy Research Programme under National Research Foundation of Singapore for their research grant (grant no. NRF2007EWT-CERP01-0420) support for this work. We would also like to thank CESEL and Facts for the use of AFM, FESEM and TEM.

Appendix A. Supplementary data

Supplementary data associated with this article can be found, in the online version, at http://dx.doi.org/10.1016/j.apcatb.2013.01.014.

References

[1] M. Elimelech, W.A. Phillip, Science 333 (2011) 712–717.
[2] M.A. Shannon, P.W. Bohn, M. Elimelech, J.G. Georgiadis, B.J. Marinas, A.M. Mayes, Nature 452 (2008) 301–310.
[3] S. Kaur, R. Gopal, W.J. Ng, S. Ramakrishna, T. Matsuura, MRS Bulletin 33 (2008) 21–26.
[4] Z. Wu, D. Zhao, Chemical Communications 47 (2011) 3332–3338.
[5] M.M. Pendergast, E.M.V. Hoek, Energy and Environental Science 4 (2011) 1946–1971.
[6] H.W. Liang, X. Cao, W.J. Zhang, H.T. Lin, F. Zhou, L.F. Chen, S.H. Yu, Advanced Functional Materials 21 (2011) 3851–3858.
[7] Y. Liu, Z. Wu, X. Chen, Z. Shao, H. Wang, D. Zhao, Journal of Materials Chemistry 22 (2012) 11908–11911.
[8] D. Rana, T. Matsuura, Chemical Reviews 110 (2010) 2448–2471.
[9] J. Mansouri, S. Harrisson, V. Chen, Journal of Materials Chemistry 20 (2010) 4567–4586.
[10] B. Van Der Bruggen, C. Vandecasteele, T. Van Gestel, W. Doyen, R. Leysen, Environmental Progress 22 (2003) 46–56.
[11] X. Zhang, T. Zhang, J. Ng, D.D. Sun, Advanced Functional Materials 19 (2009) 3731–3736.
[12] H. Choi, A.C. Sofranko, D.D. Dionysiou, Advanced Functional Materials 16 (2006) 1067–1074.
[13] H. Bai, Z. Liu, D.D. Sun, Chemical Communications 46 (2010) 6542–6544.
[14] X. Zhang, A.J. Du, P. Lee, D.D. Sun, J.O. Leckie, Journal of Membrane Science 313 (2008) 44–51.
[15] J.H. Pan, X. Zhang, A.J. Du, D.D. Sun, J.O. Leckie, Journal of the American Chemical Society 130 (2008) 11256–11257.
[16] L. Zhu, L. Gu, Y. Zhou, S. Cao, X. Cao, Journal of Materials Chemistry 21 (2011) 12503–12510.
[17] L. Liu, Z. Liu, H. Bai, D.D. Sun, Water Research 46 (2012) 1101–1112.
[18] Z. Liu, D.D. Sun, P. Guo, J.O. Leckie, Nano Letters 7 (2007) 1081–1085.
[19] H. Choi, E. Stathatos, D.D. Dionysiou, Desalination 202 (2007) 199–206.
[20] X.B. Ke, H.Y. Zhu, X.P. Gao, J.W. Liu, Z.F. Zheng, Advanced Materials 19 (2007) 785–790.
[21] X. Chen, S.S. Mao, Chemical Reviews 107 (2007) 2891–2959.
[22] K.S. Novoselov, A.K. Geim, S.V. Morozov, D. Jiang, Y. Zhang, S.V. Dubonos, I.V. Grigorieva, A.A. Firsov, Science 306 (2004) 666–669.
[23] P. Gao, J. Liu, S. Lee, T. Zhang, D.D. Sun, Journal of Materials Chemistry 22 (2012) 2292–2298.
[24] J. Liu, H. Bai, Y. Wang, Z. Liu, X. Zhang, D.D. Sun, Advanced Functional Materials 20 (2010) 4175–4181.
[25] X. Huang, X. Qi, F. Boey, H. Zhang, Chemical Society Reviews 41 (2012) 666–686.
[26] X.Y. Zhang, H.P. Li, X.L. Cui, Y. Lin, Journal of Materials Chemistry 20 (2010) 2801–2806.
[27] H. Zhang, X. Lv, Y. Li, Y. Wang, J. Li, ACS Nano 4 (2010) 380–386.
[28] S. Ding, J.S. Chen, D. Luan, F.Y.C. Boey, S. Madhavi, X.W. Lou, Chemical Communications 47 (2011) 5780–5782.
[29] J. Zhang, Z. Xiong, X.S. Zhao, Journal of Materials Chemistry 21 (2011) 3634–3640.
[30] W.S. Hummers, R.E. Offeman, Journal of the American Chemical Society 80 (1958), 1339-1339.
[31] J. Liu, H. Jeong, K. Lee, J.Y. Park, Y.H. Ahn, S. Lee, Carbon 48 (2010) 2282–2289.
[32] J. Ye, W. Liu, J. Cai, S. Chen, X. Zhao, H. Zhou, L. Qi, Journal of the American Chemical Society 133 (2011) 933–940.
[33] S. Xu, J. Ng, X. Zhang, H. Bai, D.D. Sun, Colloids and Surfaces A: Physicochemical and Engineering Aspects 379 (2011) 169–175.
[34] C.Y. Tang, Y.N. Kwon, J.O. Leckie, Journal of Membrane Science 290 (2007) 86–94.
[35] H.I. Kim, G.H. Moon, D. Monllor-Satoca, Y. Park, W. Choi, Journal of Physical Chemistry C 116 (2012) 1535–1543.
[36] S. Park, R.S. Ruoff, Nature Nanotechnology 4 (2009) 217–224.
[37] J.Y. Liao, B.X. Lei, D.B. Kuang, C.Y. Su, Energy and Environmental Science 4 (2011) 4079–4085.
[38] J.S. Chen, C. Chen, J. Liu, R. Xu, S.Z. Qiao, X.W. Lou, Chemical Communications 47 (2011) 2631–2633.
[39] H.B. Wu, H.H. Hng, X.W.D. Lou, Advanced Materials 24 (2012) 2567–2571.
[40] P. Gao, J. Liu, T. Zhang, D.D. Sun, W. Ng, Journal of Hazardous Materials 229–230 (2012) 209–216.
[41] S. Guo, S. Dong, Chemical Society Reviews 40 (2011) 2644–2672.
[42] S. Park, J. An, I. Jung, R.D. Piner, S.J. An, X. Li, A. Velamakanni, R.S. Ruoff, Nano Letters 9 (2009) 1593–1597.
[43] W. Yuan, A.L. Zydney, Journal of Membrane Science 157 (1999) 1–12.
[44] T. Zhang, J. Liu, D.D. Sun, RSC Advances 2 (2012) 5134–5137.
[45] J. Wiszniowski, D. Robert, J. Surmacz-Gorska, K. Miksch, J.-V. Weber, Photochemistry and Photobiology A: Chemistry 152 (2002) 267–273.
[46] A.W. Zularisam, A.F. Ismail, R. Salim, Desalination 194 (2006) 211–231.
[47] J. Yu, T. Ma, S. Liu, Physical Chemistry Chemical Physics 13 (2011) 3491–3501.
[48] Q. Xiang, J. Yu, M. Jaroniec, Nanoscale 3 (2011) 3670–3678.
[49] J. Liu, L. Liu, H. Bai, Y. Wang, D.D. Sun, Applied Catalysis B: Environmental 106 (2011) 76–82.